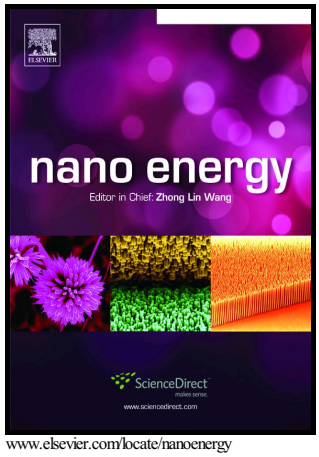

www.elsevier.com/locate/nanoenergy

Edge-Rich MoS_2 Grown on Edge-Oriented Three-dimensional Graphene Glass for High-Performance Hydrogen Evolution

Xuanhua Li, Shaohui Guo, Wei Li, Xingang Ren, Jie Su, Qiang Song, Ana Jorge Sobrido, Bingqing Wei

PII: S2211-2855(18)30949-2
DOI: https://doi.org/10.1016/j.nanoen.2018.12.044
Reference: NANOEN3292

To appear in: *Nano Energy*

Received date: 27 September 2018
Revised date: 10 December 2018
Accepted date: 13 December 2018

Cite this article as: Xuanhua Li, Shaohui Guo, Wei Li, Xingang Ren, Jie Su, Qiang Song, Ana Jorge Sobrido and Bingqing Wei, Edge-Rich MoS_2 Grown on Edge-Oriented Three-dimensional Graphene Glass for High-Performance Hydrogen Evolution, *Nano Energy,* https://doi.org/10.1016/j.nanoen.2018.12.044

Edge-Rich MoS_2 Grown on Edge-Oriented Three-dimensional Graphene Glass for High-Performance Hydrogen Evolution

Xuanhua Li[a,b,*], Shaohui Guo[a], Wei Li[a], Xingang Ren[c], Jie Su[d], Qiang Song[a], Ana Jorge Sobrido[b, e], Bingqing Wei[a,b,f,*]

[a] State Key Laboratory of Solidification Processing, Center for Nano Energy Materials, School of Materials Science and Engineering, Northwestern Polytechnical University and Shaanxi Joint Lab of Graphene (NPU), Xi'an, 710072, China

[b] Northwestern Polytechnical University-Queen Mary University of London (NPU-QMUL) Joint Research Institute of Advanced Materials and Structures (JRI-AMAS), Xi'an, 710072, China.

[c] Key Laboratory of Intelligent Computing & Signal Processing, Ministry of Education, Anhui University, Hefei, 230039, China.

[d] Wide Bandgap Semiconductor Technology Disciplines State Key Laboratory, School of Microelectronics, Xidian University, Xi'an, 710071, China.

[e] School of Engineering and Materials Science, Queen Mary University of London, Mile End Road, London E1 4NS, England.

[f] Department of Mechanical Engineering, University of Delaware, Newark, DE 19716, USA.

lixh32@nwpu.edu.cn

weib@udel.edu

Abstract:

The more exposures of the photocatalytically active sites are one of the essential elements to achieve high photocatalytic efficiency. Through the architecture designs, we have proposed an edge-rich MoS_2 nanoarray grown on an edge-oriented three-dimensional (3D) graphene (termed as the 3D-graphene/E-MoS_2) *via* chemical vapor deposition. Unlike the two-dimensional (2D) graphene, the highly conductive and transparent 3D graphene film has been grown at oblique angles on glass (*i.e.*, a graphene glass), providing the large exposed surface area for the loading of more photocatalysts. Then, the abundant photocatalytically active sites can be achieved in the subsequently deposited edge-rich MoS_2 nanoarrays, which are significantly beneficial for photocatalytic hydrogen production. The theoretical and experimental studies

have revealed the new finding in the substantial improvements of both optical and electrical properties based on the geometrically designed 3D-graphene/E-MoS_2 structures. Optically, the excellent light absorption (wavelength range: 300–800 nm) is observed, which is attributed to the favorable energy band for the efficient charge transfer between the electronically interconnected graphene and MoS_2, and orientation of the MoS_2 crystal face array. Electrically, the edge-rich MoS_2 grown on the edge-oriented 3D graphene glass can achieve the optimized charge transport along the 2D vector plane from MoS_2 layers to graphene. Consequently, the new hybrid nanostructures exhibit excellent performance as an effective photocatalyst for hydrogen generation from photocatalytic water splitting. The measured hydrogen evolution rate (2232.7 μmol/g/h) under white-light illumination is one of the highest among those photocatalysts reported to date.

Graphical abstract

fx1

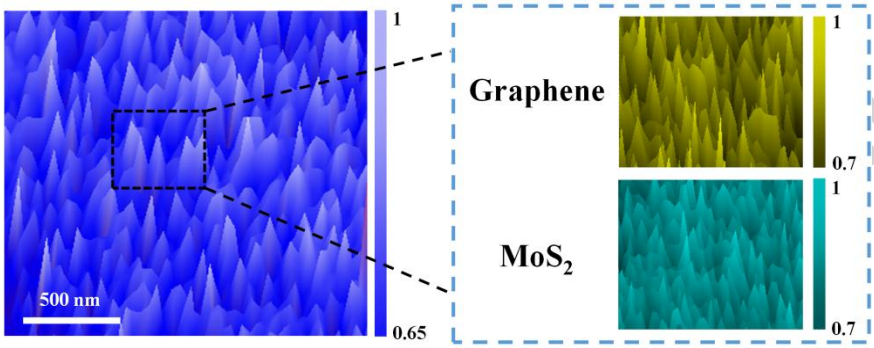

Keywords: MoS_2; graphene; hydrogen evolution; optical effect; electrical effect

1. Introduction

Over the past decades, semiconductor-based photocatalysts have attracted great attention because of their applications in solar energy conversion and environmental remediation [1-7]. Two-dimensional (2D) semiconducting transition metal dichalcogenides (TMDs), e.g., MoS_2, have gained increasing attention as an emerging class of new materials because of their unique optical and electrical properties [8-14]. The edges of the layered materials constitute the active sites for many important catalytic reactions [15-18], including

hydrodesulfurization, hydrogen evolution reaction, oxygen reduction reaction, and methane conversion [19-24]. To maximize the exposure of active edge sites and improve the overall activity, significant progress has been made in nanostructuring MoS_2 by creating nanospheres, nanoflowers, and nanosheet films [19, 20, 25, 26]. However, a high density of edge exposure is usually difficult because of their inherently high surface energy. Therefore, increasing the edge dimensions of TMDs remains a challenge.

With regard to graphene nanosheets, various synthesis methods have been reported to produce graphene nanosheets, including chemical reduction of graphene oxide, liquid exfoliation of graphite, and chemical vapor deposition (CVD) [7, 27, 28]. Among these techniques, CVD offers unique advantages for achieving uniform graphene films on metallic substrates in a controllable manner. The use of three-dimensional (3D) structures is more prevalent than the use of 2D structures in photocatalytic systems because 3D structures with less aggregation maintain the superior intrinsic properties of graphene sheets, such as their large surface area, novel physical properties, and high structural stability [29, 30]. Chen's group prepared 3D dentate graphene film using a Ni-foam template [29]. However, such a route requires costly metal substrates and the additional transfer for transparent electrodes can hinder the performance of a graphene device. Thus, direct growth of graphene on glass (*i.e.*, a graphene glass) has become an important topic [31-34]. Although Liu's group successfully synthesized monolayer graphene on the glass [35, 36], a graphene nanosheet-assembled 3D dentate architecture on glass has not been systematically studied. In the present work, an edge-oriented graphene nanosheet-assembled 3D dentate architecture (termed as the 3D-graphene) is directly grown on a glass surface without a template. This nanostructured design exhibits a large surface area and novel electron transfer properties; thus, it is a promising graphene glass for photocatalytic reactions.

Recently, TMD-based heterostructures have been extensively investigated as an efficient catalyst with active sites toward the hydrogen evolution reaction [8, 37-43]. Among these heterostructures, the graphene-MoS_2 nanohybrids have attracted extensive interest [44-53]. From the viewpoint of fabrication, the preparation of graphene-MoS_2 hybrids by simply placing MoS_2 nanosheets on top of a graphene nanosheet surface has recently been reported [43]. 3D hierarchical ternary hybrid graphene-MoS_2 composites based on

carbon nanotubes have been fabricated *via* a chemical method as catalysts for the hydrogen evolution reaction [54]. In addition, multilayer van der Waals heterostructures assembled by graphene and MoS_2 have shown good charge separation and transfer through theoretical study [42]. Unfortunately, the photocatalytic efficiency of these heterostructures is still low because of their suboptimal architectures [40, 52, 53]. A desirable platform should offer versatile benefits, such as a large surface area, preferentially exposed active sites, optimized charge transport, and broadband and strong light absorption.

In this work, we design and synthesize an edge-rich MoS_2 array grown on edge-oriented graphene glass (termed as the 3D-graphene/E-MoS_2; see Fig. 1) *via* CVD as an excellent photocatalyst for the hydrogen evolution reaction. Two major contributions have been achieved in the proposed hybrid nanostructure. Firstly, the graphene with an edge-oriented dentate architecture grown on an ordinary transparent insulating glass maintains the superior intrinsic properties of the 3D graphene, enabling the fabrication of transparent glass electrodes with a large surface area and good structural stability. Furthermore, the edge-rich MoS_2 nanosheets exhibit preferentially exposed active sites, broadband and strong light absorption, and optimized charge transport along the 2D vector plane. As a result, the hybrid nanostructures exhibit outstanding advantages as a new effective white-light photocatalyst for water splitting, with a hydrogen evolution rate of 2232.7 μmol g^{-1} h^{-1}, which is one of the highest values reported to date for a photocatalyst.

2. Results and Discussion

2.1 Preparation of 3D-Graphene/E-MoS_2

The preparation process of 3D-graphene/E-MoS_2 is illustrated in Fig. 1a and detailed in the Experimental Section. First, 3D-graphene was grown on a glass substrate using ethanol and H_2O as a precursor *via* the plasma-enhanced CVD (PECVD). Nanopits formed on the glass surface due to the etch of plasma and H_2O function as nucleation sites for graphene sheets and promoted their growth [55]. After 1 h of reaction, edge-oriented graphene sheets grew on the glass surface at an upward oblique angle. Scanning electron microscopy (SEM) and transmission electron microscopy (TEM) images of the 3D-graphene reveal that the silky nanosheets intertwisted (Fig. S1 and S2). Fig. S2c shows the in-plane structures of the 3D-graphene. Second, MoO_3 was evaporated on top of the 3D-graphene for the preparation of MoS_2. After sulfidization of

MoO_3, the 3D-graphene/E-MoS_2 configuration was obtained. The morphology of the 3D-graphene/E-MoS_2 is similar to that of the 3D-graphene, where the dense and wavy nanostructure is uniformly distributed on the glass surface (Fig. 1b). The few-layered MoS_2 nanoflakes cannot be observed in the SEM images because of their small size. The elemental mapping images of the hybrid structures in Fig. 1b indicate that the nanoflake material comprises C, Mo, and S without any impurity. The TEM images (Fig. 1c and Fig. 1d) show the nanostructures grown at oblique angles on the surface of the glass. The high-resolution TEM image of 3D-graphene/E-MoS_2 in Fig. 1e shows that dense MoS_2 is grows on the graphene surface. A line profile taken from the white line (inset in Fig. 1e) indicates a MoS_2 lattice constant of 0.62 nm. The selected-area electron diffraction (SAED) pattern in Fig. 1e demonstrates that MoS_2 has a polycrystalline nanostructure.

Raman spectra were recorded to study the structure of the 3D-graphene and 3D-graphene/E-MoS_2 samples. As shown in Fig. 2a, the characteristic peaks of the 3D-graphene are observed, including the G band at 1580 cm^{-1}, the 2D band at 2680 cm^{-1}, and the defect-related D band at 1350 cm^{-1} [56, 57]. The intensity ratio of the D band to G band (I_D/I_G) is approximately 0.5, indicating that abundant wrinkle and edge structures exist in the 3D-graphene [7, 42], consistent with the SEM and TEM observations (Fig. S1 and Fig. S2). The graphene nanosheets are uniformly distributed on the glass, as confirmed by the Raman mapping of the 3D-graphene in Fig. 2b. For the 3D-graphene/E-MoS_2 sample, in addition to the three typical peaks of graphene, two more peaks, *i.e.*, the out-of-plane Mo-S phonon mode (A^1_g) at 402 cm^{-1} and the in-plane Mo-S phonon mode (E^1_{2g}) at 376 cm^{-1}, are observed, indicating the presence of MoS_2 (Fig. 2c. The Raman peak of MoS_2 corresponding to the A^1_g mode is preferentially excited for edge-terminated structures because of polarization dependence, whereas the E^1_{2g} mode is preferentially excited for terrace-terminated structures, as illustrated in Fig. 2d [41, 43]. Accordingly, the integrated intensity ratio of the two Raman modes (E^1_{2g}:A^1_g) provides information on the structural edge termination of MoS_2. A smaller ratio reflects more edge-terminated structures. For the MoS_2 grown on graphene in the hybrid nanostructures, this ratio is approximately 30%, while it is approximately 100% of the horizontal MoS_2 nanosheets (Fig. S3). This interesting finding further corroborates that the MoS_2 nanosheets in the hybrid nanostructure have more

edge-terminated structures, consistent with the TEM observations (Fig. 1e). Furthermore, the increase in the I_D/I_G ratio from 0.5 for 3D-graphene to 0.75 for 3D-graphene/E−MoS_2 is attributed to the increase of in-plane defects in graphene and the interface generated between graphene and MoS_2 [58, 59]. In addition, the D, G, and a 2D band of graphene observed in the hybrid nanostructure are shifted to 1341, 1577, and 2691 cm^{-1}, respectively, indicating a substantial increase in the interface between graphene and MoS_2 [58, 59]. Fig. 2e and Fig. 2f present the Raman mapping images of 3D-graphene/E-MoS_2. The Raman mapping image in Fig. 2e shows that graphene (blue) and MoS_2 (white) are uniformly distributed within the hybrid nanostructures.

2.2 Photocatalytic Reaction of 3D-Graphene/E-MoS_2

Fig. 3a shows the measurement set-up of the photoelectrochemical (PEC) photocatalytic experiment. Notably, the 3D-graphene nanosheets exhibit a good electrical conductivity, with a low resistance of 70.6 Ω/sq (Fig. S4); they also exhibit high transparency, with a transmittance of nearly 88% in the wavelength range 300-900 nm (see the photos of 3D-graphene in Fig. 1 a, and the absorption of 3D-graphene in Fig. 4a). These results indicate that the 3D-graphene nanosheets can be directly used as an indium tin oxide/fluorine-doped tin oxide (ITO/FTO)-free electrode in photocatalytic tests. For comparison, several other samples, including edge-rich MoS_2 layers grown on FTO glass (termed as the E-MoS_2), edge-rich MoS_2 layers grown on a monolayer graphene (termed as the 2D-graphene/E-MoS_2), and layered and interwoven MoS_2 nanospheres synthesized using a hydrothermal method (termed as the MoS_2-spheres), were also prepared and evaluated under the same conditions (see the Experimental Section for the preparation of the samples). The magnified TEM image of the edge-rich MoS_2 grown on FTO glass is displayed in Fig. S5, and the morphology of the MoS_2-sphere sample is shown in Fig. S6.

The photocatalytic hydrogen production activities over the samples were measured without applying a bias voltage, and the Na_2SO_3 was selected as the sacrificial agent. The yield of hydrogen production is presented in Fig. 3b. Clearly, the MoS_2 spheres show the weakest photocatalysis activity among the investigated samples, with a hydrogen yield of approximately 1239.1 μmol g^{-1}. The photocatalytic activity of E-MoS_2 is relatively higher than that of the MoS_2 spheres, as reflected by the yield of hydrogen

decreasing from 2037.8 μmol g^{-1} at the first cycle to 1746.5 μmol g^{-1} after the third cycle. In comparison, the yield of hydrogen for the 2D-graphene/E-MoS_2 sample is approximately 2934.4 μmol g^{-1} in the first cycle, which is 1.44 times higher than that of the E-MoS_2 array sample. For the 3D-graphene/E-MoS_2 sample, the photocatalytic activities of hydrogen generation are further enhanced, with a hydrogen yield of approximately 4465.4 μmol g^{-1} in the first cycle, which is 3.45 times higher than that of the MoS_2-spheres sample. Correspondingly, the hydrogen evolution activity rate in the first reaction is approximately 2232.7 μmol g^{-1} h^{-1} and approximately 2104.5 μmol g^{-1} h^{-1} after a 360 min test. For the sake of clarification, the photocatalytic activities of the 3D-graphene and horizontal 2D-graphene were also measured under the same conditions. No trace amount of H_2 gas was detectable (Fig. S7 and Fig. S8).

The 3D-graphene/E-MoS_2 sample, with a hydrogen evolution rate of 2232.7 μmol/g/h under white light, exhibits the best water splitting performance in terms of yield and stability among the photocatalysts reported to date. In comparison with photocatalysts that achieve hydrogen production with several cycles, such as Sb-SnO_2 [60], CdS/Nb_2O_5/N-doped graphene [61], 5-wt.% MoS_2 quantum dots/UiO-66-NH_2/graphene [52], TiO_2/graphene [62], microwave-g-C_3N_4 [63], g-C_3N_4/$Ca_2Nb_2TaO_{10}$ [64], phosphorus-doped C_3N_4 [65], T-C_3N_4 [66], g-C_3N_4 [67], Au@MoS_2-ZnO [25], and Au multimers@MoS_2 [26], 3D-graphene/E-MoS_2 evolves hydrogen at a higher rate (Fig. 3c). 3D-graphene/E-MoS_2 also exhibits greater stability than the photocatalysts above. Hence, the as-proposed photocatalyst possesses outstanding advantages as a new effective white-light photocatalyst for water splitting.

Exploiting the practicability of our photocatalyst, we designed an integrated perovskite solar cell (PSC)/photocatalyst cell with a parallel connection in which the hydrogen evolution rate from water splitting can be enhanced based on the "new" bias voltage from the solar cell [68]. As shown in Fig. 3d, PSC was chosen because it offers a stable bias voltage on the photocatalyst device; thus, more photogenerated electrons can participate in the hydrogen evolution reaction. The PSC was placed side by side and connected in parallel with wires to the immersed catalyst electrodes. Under simulated AM 1.5G solar irradiation (100 mW cm^{-2}), the PSC had a short-circuit photocurrent density, open-circuit voltage, and fill factor of 18.12 mA cm^{-2}, 1.067 V, and 0.69, respectively. The current density-voltage (*J*–*V*) characteristic of a

representative PSC/photocatalyst parallel cell is shown in Fig. 3e, indicating that the current density of the photocatalyst combined with the solar cell is enhanced approximately four folds compared to that of the photocatalyst without the solar cell. The performance of the device under chopped AM 1.5G illumination is shown in Fig. 3f wherein the current is measured as a function of time in a two-electrode setup. The photocurrent of the parallel cell is approximately 11 mA cm^{-2}, whereas that in the photocatalyst device is approximately 3.5 mA cm^{-2}; this enhancement by the parallel cell is beneficial to the hydrogen evolution reaction.

2.3 Optical Properties of 3D-Graphene/E-MoS_2

It is necessary to understand the underlying fundamentals of the excellent photocatalytic performance of the 3D-graphene/E-MoS_2. Because the photocatalytic reaction involves both optical and electrical processes, we first investigated the absorption of 3D-graphene/E-MoS_2 along with the other four control samples: MoS_2-spheres, E-MoS_2, 3D-graphene, and 2D-graphene/E-MoS_2, as shown in Fig. 4a. The 3D-graphene sample exhibits little visible-light absorption, while the MoS_2-spheres sample exhibits strong absorption in the wavelength range of 500-800 nm, which is consistent with the results of the previous study [20]. Regarding E-MoS_2, interestingly, the broadband absorption is observed at 300-800 nm, and a strong absorption region at approximately 300-500 nm exists in comparison with that of the MoS_2-spheres sample. Furthermore, after the introduction of E-MoS_2 to 2D-graphene or 3D-graphene as a hybrid nanostructure (*i.e.*, 2D-graphene/E-MoS_2 and 3D-graphene/E-MoS_2), a similar absorption region at approximately 300-800 nm is observed with intensity decreasing in the order of 3D-graphene/E-MoS_2, 2D-graphene/E-MoS_2, and E-MoS_2.

To clarify the origin of the ultra-broadband absorption enhancement and additional absorption region at approximately 300-500 nm in the absorption spectra of E-MoS_2, 2D-graphene/E-MoS_2, and 3D-graphene/E-MoS_2, we investigated the energy band of E-MoS_2 (Fig. 4b). The light absorption at approximately 600-800 nm is ascribed to band-edge A/B excitons, and the high-energy C excitons due to the band nesting effect contribute the additional absorption at 300-500 nm (Fig. 4b and Fig. 4c) [41]. When MoS_2 nanosheets were placed on top of the graphene substrate, the oscillator strengths of the high-energy C excitons increase at approximately 422 nm, which is further verified by the extracted absorption based on the Density Functional

Theory (DFT) simulation (Fig. 4d) [69]. This phenomenon arises from the favorable energy band for the efficient charge transfer between the electronically interconnected graphene and MoS_2, which will deliver absorption enhancement particularly for the high-energy C-exciton associated with the banding nesting effect [41, 70]. Furthermore, the absorption of 3D-graphene/E-MoS_2 stronger than that of 2D-graphene/E-MoS_2 is mainly attributed to the edge-oriented 3D-graphene having a sufficiently large specific surface area to permit the loading of MoS_2 (see the calculation of surface area in Experimental Section) and more interaction between graphene and MoS_2 in 3D-graphene/E-MoS_2 (*i.e.*, more efficient charge transfer).

In addition, the large difference in the optical responses of the MoS_2-containing samples is attributed to the difference in the orientations of the MoS_2 crystal face arrays (Fig. 4e and Fig. 4f). The as-prepared edge-rich MoS_2 sample (*i.e.*, E-MoS_2) shows an aligned film in the present work (Fig. 1e). In contrast, the MoS_2 sphere prepared using the hydrothermal method exhibits disordered characteristics (Fig. S6). For ordered MoS_2, the enhanced absorption is attributed to the excitation of the collective optical resonance, which can be readily recognized by the field distribution of the electric field (Fig. 4e). The positive and negative fields are symmetrically localized at both sides of the MoS_2 surface in the vertical direction. The characteristic of symmetrical field profiles will induce polarized surface charges at the aligned E-MoS_2 surface and produce a collective optical resonance, resulting in a considerable enhancement in E-MoS_2 optical absorption at 300-500 nm. For MoS_2 spheres prepared using the hydrothermal method, there is no clear feature of the excited optical mode in the absorption spectra (Fig. 4g) and the corresponding near-field distribution (Fig. 4f). Therefore, this new absorption region at approximately 300-500 nm can be attributed to the favorable energy band in the 3D-graphene/E-MoS_2, and the aligned MoS_2 assemble.

Fig. 4h presents the external quantum efficiency (EQE) spectra of the involved samples, including the MoS_2-spheres, E-MoS_2, 2D-graphene/E-MoS_2, and 3D-graphene/E-MoS_2 samples. The MoS_2-sphere sample only exhibits a good quantum efficiency at 600-800 nm. In contrast, the E-MoS_2 and 2D-graphene/E-MoS_2 photocatalysts show good quantum efficiencies in the range 300-800 nm, with maximum EQEs of approximately 13.6% and 16.1%, respectively, at 422 nm. The 3D-graphene/E-MoS_2 sample presents a similar tendency and exhibits an EQE of 27.5% at 422 nm in Fig. 4h, which is also greater than the EQE of

the MoS_2-spheres, E-MoS_2, and 2D-graphene/E-MoS_2 samples in the spectral range from 300 to 800 nm. When comparing the EQE values and absorption plots (Fig. 4a and Fig. 4h), we observe that the wavelength regions where the absorption increases strongly match with the regions where the EQE increases. These similar behaviors of EQE and absorption indicate that the EQE enhancement partially arises from the absorption enhancement. The EQE is determined by two contributors: optical absorption and electrical effects. To investigate whether the electrical effects contribute to the EQE enhancement, we deduced the internal quantum efficiency (IQE) data reflecting the electrical effects from the EQE and absorption (Fig. 4a and Fig. 4h, respectively), and the results are presented in Fig. 4i. The IQE curves gradually increase for the MoS_2-spheres, E-MoS_2, 2D-graphene/E-MoS_2, and 3D-graphene/E-MoS_2 samples, indicating that the EQE enhancement also originates from the electrical enhancement.

2.4 Electrical properties of 3D-Graphene/E-MoS_2

Two PEC characterizations and photoluminescence (PL) analyses were performed to investigate the electrical effects, including exciton separation and carrier transport. Fig. 5a displays the photocurrent density-time (*I–t*) curves of the 3D-graphene/E-MoS_2, 2D-graphene/E-MoS_2, MoS_2-spheres, and E-MoS_2 samples under white-light illumination. The 3D-graphene/E-MoS_2 sample shows the highest photocurrent, which is 3.4, 2.8, and 1.8 times higher than those of the MoS_2-spheres, E-MoS_2 array, and 2D-graphene/E-MoS_2 samples, respectively. Fig. 5b presents the electrochemical impedance spectroscopy (EIS) Nyquist plots of the four samples under white-light irradiation. The Nyquist plots for all four samples show semicircles at high frequencies. The smallest arc radius is that of the 3D-graphene/E-MoS_2 sample, which implies the fastest interfacial electron transfer compared to that of the 2D-graphene/E-MoS_2, E-MoS_2, and MoS_2-sphere samples.

In addition, the most efficient exciton separation and charge carrier transfer occur over the 3D-graphene/E-MoS_2 sample, as further verified by the PL analysis, which is often used to study surface processes involving the photoexcited energy and electron transfer and recombination. As shown in Fig. 5c, clear emission peaks are observed at 689.5 and 708 nm for the MoS_2-sphere sample and 689 and 707 nm for the E-MoS_2 sample; this finding is in good agreement with the literature data [26]. Interestingly, with the

introduction of graphene, the intensity at 689 nm is suppressed under the excitation of a 480-nm Xe lamp light. The peak at 707 nm is quenched based on the excellent electron transport of graphene. The substantial decrease in the relative PL peak intensity in the 3D-graphene/E-MoS_2 sample further indicates that the 3D-graphene/E-MoS_2 exhibits the most outstanding electrical effects among the investigated samples.

The projected density of states and the charge density difference image were constructed through first-principles calculations to further reveal the electric properties in detail. A more intuitive understanding can be obtained from the charge density difference image in Fig. 5d. The accumulation and depletion of electrons mostly occur at the interface region; the overall direction of such transfers is from MoS_2 to graphene, as indicated by the arrow. The density of states of MoS_2 from the heterostructures reveals that the energy bands of MoS_2 in heterostructures move to the low energy states and the conduction band (CB) gets electrons easier than the pristine MoS_2 nanosheets. Thus, the electrons filling the CB of MoS_2 from heterostructures are more than those that filling the CB of the pristine MoS_2 nanosheets (Fig. 5e). The photo-induced electrons transfer along the E-MoS_2 nanosheets and then to the 3D-graphene nanosheets (Fig. 5f). Based on the optical and electrical results, we propose a mechanism of photocatalytic reaction for the hybrid nanostructure. As shown in Fig. 6, the MoS_2 sample, which exhibits broadband and strong light absorption in the wavelength range of 300-800 nm, will produce a considerable number of photoexcitons under white-light illumination (Fig. 4). With regard to the Fermi level of graphene, which is lower than that of MoS_2, the photoexcitons generated from MoS_2 will be separated and transferred to the 3D-graphene. Because of the enhanced conductivity of 3D-graphene, there is an improvement in carrier transport and reduction in recombination (Fig. 5a-c). The photoinduced electrons then participate in the hydrogen evolution reaction at the photocatalytic active sites, and the photoinduced holes can be captured by a sacrificial agent. Because the 3D-graphene/E-MoS_2 sample exhibits strong and broadband absorption, efficient exciton separation, and good electron transport, it demonstrates the best hydrogen evolution performance among the five samples.

3. Conclusions

In summary, an edge-rich MoS_2 array grown on an edge-oriented 3D-graphene glass *via* CVD is an excellent photocatalyst for the hydrogen evolution reaction. Because the 3D-graphene grows at an upward

oblique orientation on the traditional glass as a highly conductive graphene glass, the 3D-graphene/E-MoS_2 heterostructures could be directly used as an ITO/FTO-free electrode with an excellent photocatalyst capacity. In addition, the edge-rich MoS_2 sample exhibits preferentially exposed active sites, excellent light absorption, and optimized charge transport along the 2D vector plane. As a result, the hybrid nanostructures exhibit outstanding performance: they serve as a new effective white-light photocatalyst for water splitting, with a hydrogen evolution rate of 2232.7 μmol g^{-1} h^{-1} under white light, which is one of the highest values among the photocatalysts reported to date.

4. Experimental section

4.1 Preparation of photocatalysts

3D-graphene: The glass after ultrasonic cleaning and ultraviolet ray cleaning was loaded into a PECVD system (commercial 13.56 MHz RF source, with the power of 400 W) for 3D-graphene growth at 1140 °C under 50 Pa pressure for 1 h using C_2H_5OH/H_2O as a precursor. The introduction of C_2H_5OH/H_2O into the PECVD system was realized by a digital injection with the injection rate of 0.8 ml/min. After cooling to room temperature, the 3D-graphene was obtained.

3D-graphene/E-MoS_2: The 3D-graphene substrates were firstly coated with 15-nm-thick MoO_3 film as a precursor by thermal evaporation at a low deposition rate of ~0.2 Å/s. After that, the substrates were placed at the hot center of a single-zone tube furnace. Sulfur powder (from Aladdin) was placed at the upstream side of the furnace at carefully adjusted locations to set the temperature. The tube was pumped to a base pressure of 200 Pa and flushed with Ar gas to remove residue oxygen. Subsequently, the heating center of the furnace was quickly raised to a reaction temperature of 550 °C in 30 min, and the sulfur precursor was kept at 220 °C well above their melting temperature. The furnace was held at reaction temperature for 10 min, during which Ar gas was kept flowing at a rate of 100 s.c.c.m. to transport sulfur to the substrate. After the reaction, 3D-graphene/E-MoS_2 was obtained.

E-MoS_2 and 2D-graphene/E-MoS_2: Preparation of E-MoS_2 and 2D-graphene/E-MoS_2 was similar to that of the 3D-graphene/E-MoS_2. 3D-graphene substrates were replaced by a glass substrate and horizon 2D-graphene grown on the glass for the E-MoS_2 and 2D-graphene/E-MoS_2, respectively.

MoS_2-spheres: MoS_2-spheres were obtained through the hydrothermal process [25]. In detail, Na_2MoO_4 (2.0 mmol) and L-cysteine solutions (4.0 mmol) were prepared and dispersed in 40.0 ml ultrapure water. After 20 min sonication, the solution was transferred into a 50 ml Teflon-lined stainless steel autoclave. The autoclave was heated at 200 °C for 12 h and cooled to room temperature naturally. Hereafter, the resulting samples were named as the MoS_2-spheres.

4.2 Characterization of the photocatalysts

The morphology of the samples was characterized using SEM (FEI NOVASEM) and TEM (FEI Tecnai F30G2). The absorption was measured using an UV-vis spectrophotometer (Perkin-Elmer Lambda 35 UV-VIS). The PL was examined using a PL spectrometer (FLS 980) that was equipped with a Xe lamp. The Raman spectrum was measured using a Raman spectrometer (Renishaw inVia) with a 532 nm laser. EQE measurements of the samples were performed with a 300 W Xe lamp coupled with a monochromator controlled by a computer.

4.3 Computational methods

The first-principles calculations were performed with the projector augmented wave (PAW) pseudopotential [71] and plane-wave basis set with a cutoff energy of 400 eV, implemented in the Vienna Ab-initio Simulation Package (VASP) code [72, 73]. Generalized gradient approximation (GGA) with the Perdew–Burke–Ernzerhof (PBE) functional and the van der Waals correction proposed by Grimme were employed to solve the Kohn-Sham DFT [74]. All structure relaxations were carried out until all the atomic forces on each ion are less than 0.01 $eV \cdot Å^{-1}$. The Monkhorst-Pack k-point mesh was sampled with a separation of about 0.015 $Å^{-1}$ in the Brillouin zone during the relaxation and electronic calculation periods. Dipole corrections were applied in the self-consistent calculations to eliminate the spurious interaction between the dipole moments of periodic images in the z-direction. For the 3D-graphene/E-MoS_2 model, a 5×5 graphene supercell and a 4×4 MoS_2 supercell were adopted to minimize the lattice mismatch of the sample. A vacuum region of about 15 Å normal to the interface was added to prevent interactions between periodic image slabs.

The profile of the electric field distribution was obtained through rigorously solving Maxwell's equations by finite difference method [75-77]. The edge-ordered MoS_2 in the model was vertically aligned with the width of 0.62 nm, height of 15 nm and periodicity of 1 nm. A non-uniform grid size was used in the model, and the grid size of 0.01 nm was adopted to capture the geometrical characteristics of MoS_2 in the horizontal x-direction, while the grid size of 1 nm was used in the vertical y-direction. The perfectly matched layer was adopted for truncating the simulation domain and absorbing the reflected wave at the top and bottom side. The periodic boundary condition was imposed on the right and left sides. The dielectric constant of MoS_2 was obtained from the reference [78].

4.4 Photocatalytic Activity

The photocatalytic reaction was conducted in a closed gas circulation and evacuation system. The three electrode system is used to carry out hydrogen evolution reaction with no external bias, in which the nanostructured materials as the working electrode, Pt plate as the counter electrode, and Ag/AgCl as the reference electrode. And the aqueous Na_2SO_3 solution (0.3 M) was prepared as a sacrificial agent to consume the photo-generated holes for hydrogen evolution reaction. A light source (Microsolar 300 with a 300 W Xe arc lamp) was equipped with a fan for dissipating excessive heat effectively. The average power was determined to be 0.5 W cm^{-2}. The quartz cell was placed 5.0 cm away from the lamp. During the photocatalytic reaction, the gasses evolved were transferred into a sample loop by a peristaltic pump and were further quantified using gas chromatography (Shimadzu GC-2014c), equipped with a thermal conductivity detector (TCD). The yield of hydrogen gas produced from the reactor was measured every half hour.

MoS_2 loading amount in the 3D-graphene/E-MoS_2 or 2D-graphene/2D-MoS_2 could be calculated. Every graphene sheet in the 3D-graphene can be approximated as a rectangle. As shown in Fig. 1b and Fig. 1c, the length and width is 500 nm and 150 nm, respectively. By counting, we find that there are 6 graphene sheets in the 500 nm^2 area. Thus, the graphene area in 500 nm^2 area is 500 nm ×150 nm ×6 = 450000 nm^2. For the 2D graphene, the graphene area is only 500 nm × 500 nm = 250000 nm^2 in 500 nm^2 area. Therefore, the graphene area in 3D graphene is 1.8 folds larger than that of 2D-graphene. After a 15-nm-thick MoO_3

film was coated on the graphene sheets and the MoO_3 were subsequently sulfurized to MoS_2, the MoS_2 loading in the 3D-graphene is also estimated to be 1.8 folds larger than that in the 2D-graphene.

Photoelectrochemical measurements including I-t curves and EIS Nyquist plots were performed using a three-electrode reactor, with the nanostructured materials as the working electrode, Pt plate as the counter electrode, and Ag/AgCl as the reference electrode. The electrolyte for the photoelectrochemical study was prepared with 0.3 M Na_2SO_4. The photocurrent was measured with linear-sweep voltammetry. The current intensity-time was obtained with 1.2 V bias (electrochemical workstation, Chenhua 760). The EIS at a frequency range from 100 kHz to 1 Hz was measured under light illumination.

Supporting Information

Supporting information is available in the online version of the paper.

Acknowledgments

Xuanhua Li, Shaohui Guo, and Wei Li contributed equally to this work. This research is supported by the Basic Research Fund for Free Exploration (JCYJ20170815161437298), the National Natural Science Foundation of China (51571166, 61505167, and 61701003)), and the Key Scientific and Technological Team from Shaanxi Province (No. 2015KCT-12). We thank the support of the Project of Shaanxi Young Stars in Science and Technology (2017KJXX-18), and the Research Fund of the State Key Laboratory of Solidification Processing (NWPU) (Grant No. 147-QZ-2016). This work is also supported by Natural Science Research Foundation of Anhui Province (No. 1808085QF179).

Conflict of Interest

The authors declare no conflict of interest.

References

[1] T. A. Pham, Y. Ping, G. Galli, Modelling heterogeneous interfaces for solar water splitting, Nat. Mater. 16 (2017) 401-408.

[2] J. Deng, H. B. Li, S. H. Wang, D. Ding, M. S. Chen, C. Liu, Z. Q. Tian, K. S. Novoselov, C. Ma, D. H. Deng, X. H. Bao, Multiscale structural and electronic control of molybdenum disulfide foam for highly efficient hydrogen production, Nat. Commun. 8 (2017) 14430.

[3] Q. Wang, T. Hisatomi, Q. Jia, H. Tokudome, M. Zhong, C. Wang, Z. Pan, T. Takata, M. Nakabayashi, N. Shibata, Y. Li, I. D. Sharp, A. Kudo, T. Yamada, K. Domen, Scalable water splitting on particulate photocatalyst sheets with a solar-to-hydrogen energy conversion efficiency exceeding 1%, Nat. Mater. 15 (2016) 611-615.

[4] T. T. Tong, X. H. Li, S. H. Guo, J. Han, B. Q. Wei, Sequential solvent processing with hole transport materials for improving efficiency of traditionally-structured perovskite solar cells, Nano Energy 41 (2017) 591-599.

[5] S. Wang, X. Li, T. Tong, J. Han, Y. Zhang, J. Zhu, Z. Huang, W. C. H. Choy, Spontaneous improvements in film quality and interfacial engineering for efficient perovskite solar cells, Sol. RRL 2 (2018) 1800027.

[6] X. H. Li, T. T. Tong, Q. J. Wu, S. H. Guo, Q. Song, J. Han, Z. X. Huang, Unique seamlessly bonded CNT@graphene hybrid nanostructure introduced in an interlayer for efficient and stable perovskite solar cells, Adv. Funct. Mater. 28 (2018) 1800475.

[7] A. J. Mannix, B. Kiraly, M.C. Hersam, N. P. Guisinger, Synthesis and chemistry of elemental 2D materials, Nat. Rev. Chem. 1 (2017) 0014.

[8] Y. Sun, F. Alimohammadi, D. Zhang, G. Guo, Enabling colloidal synthesis of edge-oriented MoS_2 with expanded interlayer spacing for enhanced HER catalysis, Nano Lett. 17 (2017) 1963-1969.

[9] U. Gupta, C. N. R. Rao, Hydrogen generation by water splitting using MoS_2 and other transition metal dichalcogenides, Nano Energy 41 (2017) 49-65.

[10] R. Peng, L. B. Liang, Z. D. Hood, A. Boulesbaa, A. Puretzky, A. V. Ievlev, J. Come, O. S. Ovchinnikova, H. Wang, C. Ma, M. F. Chi, B. G. Sumpter, Z. L. Wu, In-plane heterojunctions enable multiphasic two-dimensional (2D) MoS_2 nanosheets as efficient photocatalysts for hydrogen evolution from water reduction, ACS Catal. 6 (2016) 6723-6729.

[11] Y. Bai, H. N. Chen, S. Xiao, Q. F. Xue, T. Zhang, Z. L. Zhu, Q. Li, C. Hu, Y. Yang, Z. C. Hu, F. Huang, K. S. Wong, H. L. Yip, S. H. Yang, Effects of a molecular monolayer modification of NiO nanocrystal layer surfaces on perovskite crystallization and interface contact toward faster hole extraction and higher photovoltaic performance, Adv. Funct. Mater. 26 (2016) 2950-2958.

[12] J. Shi, R. Tong, X. Zhou, Y. Gong, Z. Zhang, Q. Ji, Y. Zhang, Q. Fang, L. Gu, X. Wang, Z. Liu, Y. Zhang, Temperature-mediated selective growth of MoS_2/WS_2 and WS_2/MoS_2 vertical stacks on Au foils for direct photocatalytic applications, Adv. Mater. 28 (2016) 10664-10672.

[13] Y. Li, S. Hao, J. G. DiStefano, A. A. Murthy, E. D. Hanson, Y. Xu, C. Wolverton, X. Chen, V. P. Dravid, Site-specific positioning and patterning of MoS_2 monolayers: the role of Au seeding, ACS Nano 12 (2018) 8970-8976.

[14] Y. Li, J. D. Cain, E. D. Hanson, A. A. Murthy, S. Hao, F. Shi, Q. Li, C. Wolverton, X. Chen, V. P. Dravid, Au@MoS_2 core-shell heterostructures with strong light-matter interactions, Nano Lett. 16 (2016) 7696-7702.

[15] H. Li, C. Tsai, A. L. Koh, L. Cai, A. W. Contryman, A. H. Fragapane, J. Zhao, H. S. Han, H. C. Manoharan, F. Abild-Pedersen, J. K. Norskov, X. Zheng, Activating and optimizing MoS_2 basal planes for hydrogen evolution through the formation of strained sulfur vacancies, Nat. Mater. 15 (2016) 48-53.

[16] C. Tang, L. Zhong, B. Zhang, H. F. Wang, Q. Zhang, 3D mesoporous van der Waals heterostructures for trifunctional energy electrocatalysis, Adv. Mater. 30 (2018) 1705110.

[17] Y. Li, M. B. Majewski, S. M. Islam, S. Hao, A. A. Murthy, J. G. DiStefano, E. D. Hanson, Y. Xu, C. Wolverton, M. G. Kanatzidis, M. R. Wasielewski, X. Chen, V. P. Dravid, Morphological engineering of winged Au@MoS_2 heterostructures for electrocatalytic hydrogen evolution, Nano Lett. 18 (2018) 7104-7110.

[18] X. Sun, J. Huo, Y.D. Yang, L. Xu, S. Y. Wang, The Co_3O_4 nanosheet array as support for MoS_2 as highly efficient electrocatalysts for hydrogen evolution reaction, J. Energy Chem. 26 (2017) 1136-1139.

[19] C. Liu, D. S. Kong, P. C. Hsu, H. T. Yuan, H. W. Lee, Y. Y. Liu, H. T. Wang, S. Wang, K. Yan, D. C. Lin, P. A. Maraccini, K. M. Parker, A. B. Boehm, Y. Cui, Rapid water disinfection using vertically aligned MoS_2 nanofilms and visible light, Nat. Nanotechnol. 11 (2016) 1098-1104.

[20] H. Li, H. Wu, S. Yuan, H. Qian, Synthesis and characterization of vertically standing MoS_2 nanosheets, Sci. Rep. 6 (2016) 21171.

[21] J. H. Yu, H. R. Lee, S. S. Hong, D. Kong, H. W. Lee, H. Wang, F. Xiong, S. Wang, Y. Cui, Vertical heterostructure of two-dimensional MoS_2 and WSe_2 with vertically aligned layers, Nano Lett. 15 (2015) 1031-1035.

[22] H. Wang, D. Kong, P. Johanes, J. J. Cha, G. Zheng, K. Yan, N. Liu, Y. Cui, $MoSe_2$ and WSe_2 nanofilms with vertically aligned molecular layers on curved and rough surfaces, Nano Lett. 13 (2013) 3426-3433.

[23] X. Xu, G. Zhou, X. Dong, J. Hu, Interface band engineering charge transfer for 3D MoS_2 photoanode to boost photoelectrochemical water splitting, ACS Sustain. Chem. Eng. 5 (2017) 3829-3836.

[24] G. R. Bhimanapati, T. Hankins, Y. Lei, R. A. Vila, I. Fuller, M. Terrones, J. A. Robinson, Growth and tunable surface wettability of vertical MoS_2 layers for improved hydrogen evolution reactions, ACS Appl. Mater. Inter. 8 (2016) 22190-22195.

[25] S. Guo, X. Li, J. Zhu, T. Tong, B. Wei, Au NPs@MoS_2 sub-micrometer sphere-ZnO nanorod hybrid structures for efficient photocatalytic hydrogen evolution with excellent stability, Small 12 (2016) 5692-5701.

[26] X. Li, S. Guo, C. Kan, J. Zhu, T. Tong, S. Ke, W. C. H. Choy, B. Wei, Au multimer@MoS_2 hybrid structures for efficient photocatalytical hydrogen production *via* strongly plasmonic coupling effect, Nano Energy 30 (2016) 549-558.

[27] C. Tang, B. Wang, H. F. Wang, Q. Zhang, Defect engineering toward atomic Co-N_x-C in hierarchical graphene for rechargeable flexible solid Zn-air batteries, Adv. Mater. 29 (2017) 1703185.

[28] J. M. Zhu, X.H. Li, Y.Y. Zhang, J. Wang, B.Q. Wei, Graphene-enhanced nanomaterials for wall painting protection, Adv. Funct. Mater. 28 (2018) 1803872.

[29] Z. P. Chen, W. C. Ren, L. B. Gao, B. L. Liu, S. F. Pei, H. M. Cheng, Three-dimensional flexible and conductive interconnected graphene networks grown by chemical vapor deposition, Nat. Mater. 10 (2011) 424-428.

[30] B. Li, Y. X. Zhang, X. B. Zhou, Z. L. Liu, Q. Z. Liu, X. H. Li, Different dye removal mechanisms between monodispersed and uniform hexagonal thin plate-like MgAl-CO_3^{2-}-LDH and its calcined product in efficient removal of congo red from water, J. Alloy. Compd. 673 (2016) 265-271.

[31] D. C. Wei, Y. H. Lu, C. Han, T. C. Niu, W. Chen, A. T. S. Wee, Critical crystal growth of graphene on dielectric substrates at low temperature for electronic devices, Angew. Chem. Int. Ed. 52 (2013) 14121-14126.

[32] J. Hwang, M. Kim, D. Campbell, H. A. Alsalman, J. Y. Kwak, S. Shivaraman, A. R. Woll, A. K. Singh, R. G. Hennig, S. Gorantla, M. H. Rummeli, M. G. Spencer, Van der Waals epitaxial growth of graphene on sapphire by chemical vapor deposition without a metal catalyst, ACS Nano 7 (2013) 385-395.

[33] J. Y. Chen, Y .L. Guo, L. L. Jiang, Z. P. Xu, L.P. Huang, Y. Z. Xue, D. C. Geng, B. Wu, W. P. Hu, G. Yu, Y. Q. Liu, Near-equilibrium chemical vapor deposition of high-quality single-crystal graphene directly on various dielectric substrates, Adv. Mater. 26 (2014) 1348-1353.

[34] J. Y. Chen, Y. L. Guo, Y. G. Wen, L. P. Huang, Y.Z. Xue, D. C. Geng, B. Wu, B. R. Luo, G. Yu, Y. Q. Liu, Two-stage metal-catalyst-free growth of high-quality polycrystalline graphene films on silicon nitride substrates, Adv. Mater. 25 (2013) 992-997.

[35] J. Sun, Y. Chen, M. K. Priydarshi, Z. Chen, A. Bachmatiuk, Z. Zou, Z. Chen, X. Song, Y. Gao, M. H. Rummeli, Y. Zhang, Z. Liu, Direct chemical vapor deposition-derived graphene glasses targeting wide ranged applications, Nano Lett. 15 (2015) 5846-5854.

[36] Y. B. Chen, J. Y. Sun, J. F. Gao, F. Du, Q. Han, Y. F. Nie, Z. Chen, A. Bachmatiuk, M. K. Priydarshi, D. L. Ma, X. J. Song, X. S. Wu, C. Y. Xiong, M. H. Rummeli, F. Ding, Y. F. Zhang, Z. F. Liu, Growing uniform graphene disks and films on molten glass for heating devices and cell culture, Adv. Mater. 27 (2015) 7839-7846.

[37] X. Li, J. Zhu, B. Wei, Hybrid nanostructures of metal/two-dimensional nanomaterials for plasmon-enhanced applications. Chem. Soc. Rev. 45 (2016).3145-3187.

[38] X. Zhang, Q. W. Zhang, Y. F. Sun, P. Y. Zhang, X. Gao, W. Zhang, J. X. Guo, MoS_2-graphene hybrid nanosheets constructed 3D architectures with improved electrochemical performance for lithium-ion batteries and hydrogen evolution, Electrochim. Acta 189 (2016) 224-230.

[39] A. Behranginia, M. Asadi, C. Liu, P. Yasaei, B. Kumar, P. Phillips, T. Foroozan, J.C. Waranius, K. Kim, J. Abiade, R.F. Klie, L.A. Curtiss, A. Salehi-Khojin, Highly efficient hydrogen evolution reaction using crystalline layered three-dimensional molybdenum disulfides grown on graphene film, Chem. Mater. 28 (2016) 549-555.

[40] A. Behranginia, P. Yasaei, A.K. Majee, V.K. Sangwan, F. Long, C.J. Foss, T. Foroozan, S. Fuladi, M.R. Hantehzadeh, R. Shahbazian-Yassar, M.C. Hersam, Z. Aksamija, A. Salehi-Khojin, Direct growth of high mobility and low-noise lateral MoS_2-graphene heterostructure electronics, Small 13 (2017) 1604301.

[41] L. Wang, Z. Wang, H. Y. Wang, G. Grinblat, Y. L. Huang, D. Wang, X. H. Ye, X. B. Li, Q. Bao, A. S. Wee, S. A. Maier, Q. D. Chen, M. L. Zhong, C. W. Qiu, H. B. Sun, Slow cooling and efficient extraction of C-exciton hot carriers in MoS_2 monolayer, Nat. Commun. 8 (2017) 13906.

[42] L. Xu, W. Q. Huang, W. Y. Hu, K. Yang, B. X. Zhou, A. L. Pan, G. F. Huang, Two-dimensional MoS_2-graphene-based multilayer van der Waals heterostructures: enhanced charge transfer and optical absorption, and electric-field tunable Dirac point and band gap, Chem. Mater. 29 (2017) 5504-5512.

[43] L. B. Ma, Y. Hu, G. Y. Zhu, R. P. Chen, T. Chen, H. L. Lu, Y. R. Wang, J. Liang, H. X. Liu, C. Z. Yan, Z. X. Tie, Z. Jin, J. Liu, In situ thermal synthesis of inlaid ultrathin MoS_2/graphene nanosheets as electrocatalysts for the hydrogen evolution reaction, Chem. Mater. 28 (2016) 5733-5742.

[44] Y. Zhao, X. Xie, J. Zhang, H. Liu, H. J. Ahn, K. Sun, G. Wang, MoS_2 nanosheets supported on 3D graphene aerogel as a highly efficient catalyst for hydrogen evolution, Chem. 21 (2015) 15908-15913.

[45] X. Yu, R. Du, B. Li, Y. Zhang, H. Liu, J. Qu, X. An, Biomolecule-assisted self-assembly of CdS/MoS_2/graphene hollow spheres as high-efficiency photocatalysts for hydrogen evolution without noble metals, Appl. Catal. B-Environ. 182 (2016) 504-512.

[46] S. H. Choi, Y. N. Ko, J. K. Lee, Y. C. Kang, 3D MoS_2-graphene microspheres consisting of multiple nanospheres with superior sodium ion storage properties, Adv. Funct. Mater. 25 (2015) 1780-1788.

[47] X. Wang, G. Li, M. H. Seo, F. M. Hassan, M. A. Hoque, Z. Chen, Sulfur atoms bridging few-layered MoS_2 with S-doped graphene enable highly robust anode for lithium-ion batteries, Adv. Energy Mater. 5 (2015) 1501106.

[48] Y. J. Tang, Y. Wang, X. L. Wang, S. L. Li, W. Huang, L. Z. Dong, C. H. Liu, Y. F. Li, Y. Q. Lan, Molybdenum disulfide/nitrogen-doped reduced graphene oxide nanocomposite with enlarged interlayer spacing for electrocatalytic hydrogen evolution, Adv. Energy Mater. 6 (2016) 1600116.

[49] W. Cui, S. Xu, B. Yan, Z. Guo, Q. Xu, B. G. Sumpter, J. Huang, S. Yin, H. Zhao, Y. Wang, Triphasic 2D materials by vertically stacking laterally heterostructured 2H-/1T'-MoS_2 on graphene for enhanced photoresponse, Adv. Electron. Mater. 3 (2017) 1700024.

[50] J. Wang, J. L. Liu, D. L. Chao, J. X. Yan, J. Y. Lin, Z. X. Shen, Self-assembly of honeycomb-like MoS_2 nanoarchitectures anchored into graphene foam for enhanced lithium-ion storage, Adv. Mater. 26 (2014) 7162-7169.

[51] K. Chang, Z. W. Mei, T. Wang, Q. Kang, S. X. Ouyang, J. H. Ye, MoS_2/graphene cocatalyst for efficient photocatalytic H_2 evolution under visible light irradiation, ACS Nano, 8 (2014) 7078-7087.

[52] X. Hao, Z. Jin, H. Yang, G. Lu, Y. Bi, Peculiar synergetic effect of MoS_2 quantum dots and graphene on metal-organic frameworks for photocatalytic hydrogen evolution, Appl. Catal. B-Environ. 210 (2017) 45-56.

[53] X. Wan, K. Chen, Z. Chen, F. Xie, X. Zeng, W. Xie, J. Chen, J. Xu, Controlled electrochemical deposition of large-area MoS_2 on graphene for high-responsivity photodetectors, Adv. Funct. Mater. 27 (2017) 1603998.

[54] M. Khan, A. Bin Yousaf, M.M. Chen, C. S. Wei, X. B. Wu, N. D. Huang, Z. M. Qi, L. B. Li, Molybdenum sulfide/graphene-carbon nanotube nanocomposite material for electrocatalytic applications in hydrogen evolution reactions, Nano Res. 9 (2016) 837-848.

[55] A. Cao, X. F. Zhang, C. L. Xu, J. Liang, D. H. Wu, B. Q. Wei, Aligned carbon nanotube growth under oxidative ambient, J. Mater. Res. 16 (2001) 3107-3110.

[56] K. D. Park, M. B. Raschke, J. M. Atkin, Y. H. Lee, M. S. Jeong, Probing bilayer grain boundaries in large-area graphene with tip-enhanced Raman spectroscopy, Adv. Mater. 29 (2017) 1603601.

[57] Q. Song, F. Ye, X. W. Yin, W. Li, H. J. Li, Y. S. Liu, K. Z. Li, K. Y. Xie, X. H. Li, Q. G. Fu, L. F. Cheng, L. T. Zhang, B. Q. Wei, Carbon nanotube-multilayered graphene edge plane core-shell hybrid foams for ultrahigh-performance electromagnetic-interference shielding, Adv. Mater. 29 (2017) 1701583.

[58] G. C. Huang, T. Chen, W. X. Chen, Z. Wang, K. Chang, L. Ma, F. H. Huang, D. Y. Chen, J. Y. Lee, Graphene-like MoS_2/graphene composites: cationic surfactant-assisted hydrothermal synthesis and electrochemical reversible storage of lithium, Small 9 (2013) 3693-3703.

[59] H. He, J. Lin, W. Fu, X. Wang, H. Wang, Q. Zeng, Q. Gu, Y. Li, C. Yan, B. K. Tay, C. Xue, X. Hu, S. T. Pantelides, W. Zhou, Z. Liu, MoS_2/TiO_2 edge-on heterostructure for efficient photocatalytic hydrogen evolution, Adv. Energy Mater. 6 (2016) 1600464.

[60] L. Yang, J. Huang, L. Shi, L. Cao, W. Zhou, K. Chang, X. Meng, G. Liu, Y. Jie, J. Ye, Efficient hydrogen evolution over Sb-doped SnO_2 photocatalyst sensitized by eosin Y under visible light irradiation, Nano Energy 36 (2017) 331-340.

[61] Z. Yue, A. Liu, C. Zhang, J. Huang, M. Zhu, Y. Du, P. Yang, Noble-metal-free hetero-structural CdS/Nb_2O_5/N-doped-graphene ternary photocatalytic system as visible-light-driven photocatalyst for hydrogen evolution, Appl. Catal. B-Environ. 201 (2017) 202-210.

[62] Y. Lu, B. Ma, Y. Yang, E. Huang, Z. Ge, T. Zhang, S. Zhang, L. Li, N. Guan, Y. Ma, Y. Chen, High activity of hot electrons from bulk 3D graphene materials for efficient photocatalytic hydrogen production, Nano Res. 10 (2017) 1662-1672.

[63] H. Liu, D. Chen, Z. Wang, H. Jing, R. Zhang, Microwave-assisted molten-salt rapid synthesis of isotype triazine-/heptazine based g-C_3N_4 heterojunctions with highly enhanced photocatalytic hydrogen evolution performance, Appl. Catal. B-Environ. 203 (2017) 300-313.

[64] S. Thaweesak, M. Lyu, P. Peerakiatkhajohn, T. Butburee, B. Luo, H. Chen, L. Wang, Two-dimensional g-C_3N_4/$Ca_2Nb_2TaO_{10}$ nanosheet composites for efficient visible light photocatalytic hydrogen evolution, Appl. Catal. B-Environ. 202 (2017) 184-190.

[65] S. E. Guo, Z. P. Deng, M. X. Li, B. J. Jiang, C. G. Tian, Q. J. Pan, H. G. Fu, Phosphorus-doped carbon nitride tubes with a layered micro-nanostructure for enhanced visible-light photocatalytic hydrogen evolution, Angew. Chem. Int. Ed. 55 (2016) 1830-1834.

[66] Z. W. Tong, D. Yang, Z. Li, Y. H. Nan, F. Ding, Y. C. Shen, Z. Y. Jiang, Thylakoid-inspired multishell g-C_3N_4 nanocapsules with enhanced visible-light harvesting and electron transfer properties for high-efficiency photocatalysis, ACS Nano, 11 (2017) 1103-1112.

[67] Y. N. Liu, C. C. Shen, N. Jiang, Z. W. Zhao, X. Zhou, S. J. Zhao, A. W. Xu, g-C_3N_4 hydrogen-bonding viologen for significantly enhanced visible-light photocatalytic H_2 evolution, ACS Catal. 7 (2017) 8228-8234.

[68] C. M. Ding, W. Qin, N. Wang, G. J. Liu, Z. L. Wang, P. L. Yan, J. Y. Shi, C. Li, Solar-to-hydrogen efficiency exceeding 2.5% achieved for overall water splitting with an all earth-abundant dual-photoelectrode, Phys. Chem. Chem. Phys. 16 (2014) 15608-15614.

[69] J. Mertens, Y. M. Shi, A. Molina-Sanchez, L. Wirtz, H. Y. Yang, J. J. Baumberg, Excitons in a mirror: formation of "optical bilayers" using MoS_2 monolayers on gold substrates, Appl. Phys. Lett. 104 (2014) 191105.

[70] Y. Ma, Y. Dai, M. Guo, C. Niu, B. Huang, Graphene adhesion on MoS_2 monolayer: an ab initio study, Nanoscale 3 (2011) 3883-3887.

[71] G. Kresse, D. Joubert, From ultrasoft pseudopotentials to the projector augmented-wave method, Phys. Rev. B, 59 (1999) 1758-1775.

[72] G. Kresse, Ab-initio molecular-dynamics for liquid-metals, J. Non-Cryst. Solids 193 (1995) 222-229.

[73] G. Kresse, J. Furthmuller, Efficiency of ab-initio total energy calculations for metals and semiconductors using a plane-wave basis set, Comp. Mater. Sci. 6 (1996) 15-50.

[74] S. Grimme, Semiempirical GGA-type density functional constructed with a long-range dispersion correction, J. Comput. Chem. 27 (2006) 1787-1799.

[75] Z. X. Huang, T. Koschny, C. M. Soukoulis, Theory of pump-probe experiments of metallic metamaterials coupled to a gain medium, Phys. Rev. Lett. 108 (2012) 187402.

[76] X. G. Ren, Z. X. Huang, X. L. Wu, S. L. Lu, H. Wang, L. Wu, S. Li, High-order unified symplectic FDTD scheme for the metamaterials, Comput. Phys. Commun. 183 (2012) 1192-1200.

[77] S. H. Guo, X. H. Li, X. G. Ren, L. Yang, J. M. Zhu, B. Q. Wei, Optical and electrical enhancement of hydrogen evolution by MoS_2@MoO_3 core-shell nanowires with designed tunable plasmon resonance, Adv. Funct. Mater. 28 (2018) 1802567.

[78] A. R. Beal, H. P. Hughes, Kramers-kronig analysis of the reflectivity spectra of 2H-MoS_2, 2H-$MoSe_2$ and 2H-$MoTe_2$, J. Phys. C Solid State Phys. 12 (1979) 881-890.

Dr. Xuanhua Li received his B.S. degree from the Wuhan University of Technology in 2007, and M.S. degree from USTC in 2010. After that, he started his doctoral studies and received a Ph.D. degree at the Department of Electrical and Electronic Engineering, the University of Hong Kong in 2014. After short research in the Institute of Intelligent Machines, CAS, he began his career at the Center of Nano Energy Materials, Northwestern Polytechnical University as a professor. His research is focused on the synthesis of 2D nanomaterials and novel metal NPs. He is also interested in plasmon-enhanced solar cells, photocatalytic reaction, and optical sensors.

Shaohui Guo received his B.S. degree from Northwestern Polytechnical University in 2014, and he is now an M.S. candidate at Northwestern Polytechnical University under the supervision of Professor Bingqing Wei and Professor Xuanhua Li. His current research includes the development of nanostructured materials for photocatalysis and surface-enhanced Raman scattering (SERS).

Dr. Qiang Song received his B.S. degree from Xi'an Technological University in 2007 and received a Ph.D. degree at School of Materials, Northwestern Polytechnical University in 2014. After that, he began his career at the Center of Nano Energy Materials, Northwestern Polytechnical University as an associate professor. His research is focused on the synthesis of carbon nanomaterials and their composites.

Dr. Ana Jorge Sobrido received her B.S. degree from the University of La Laguna, Spain in 2004 and Ph. D degree from Autonomous University of Barcelona, Spain, in 2009. From 2013-2016, she worked in the University College London as a postdoctoral research associate. After that, she began her career at the Queen Mary University of London as an academic fellow. She is interested in nanostructured hybrid materials for energy applications.

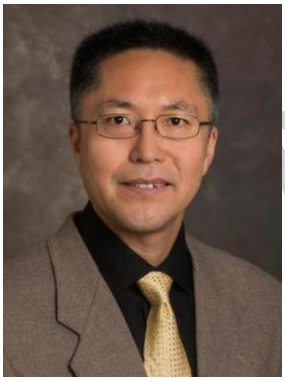

Dr. Bingqing Wei is a Professor in the Department of Mechanical Engineering at the University of Delaware, USA. He was an Assistant Professor in the Department of Electrical & Computer Engineering and Center for Computation & Technology at Louisiana State University from 2003 to 2007. From 2000 to 2003, he was a Research Scientist at Rensselaer Polytechnic Institute, Department of Materials Science and Engineering and Rensselaer Nanotechnology Center. Dr. Wei was a visiting scientist at Max-Planck-Institut

für Metallforschung, Stuttgart, Germany in 1998 and 1999. From 1992 to 2001, he was a faculty member at Tsinghua University in Beijing.

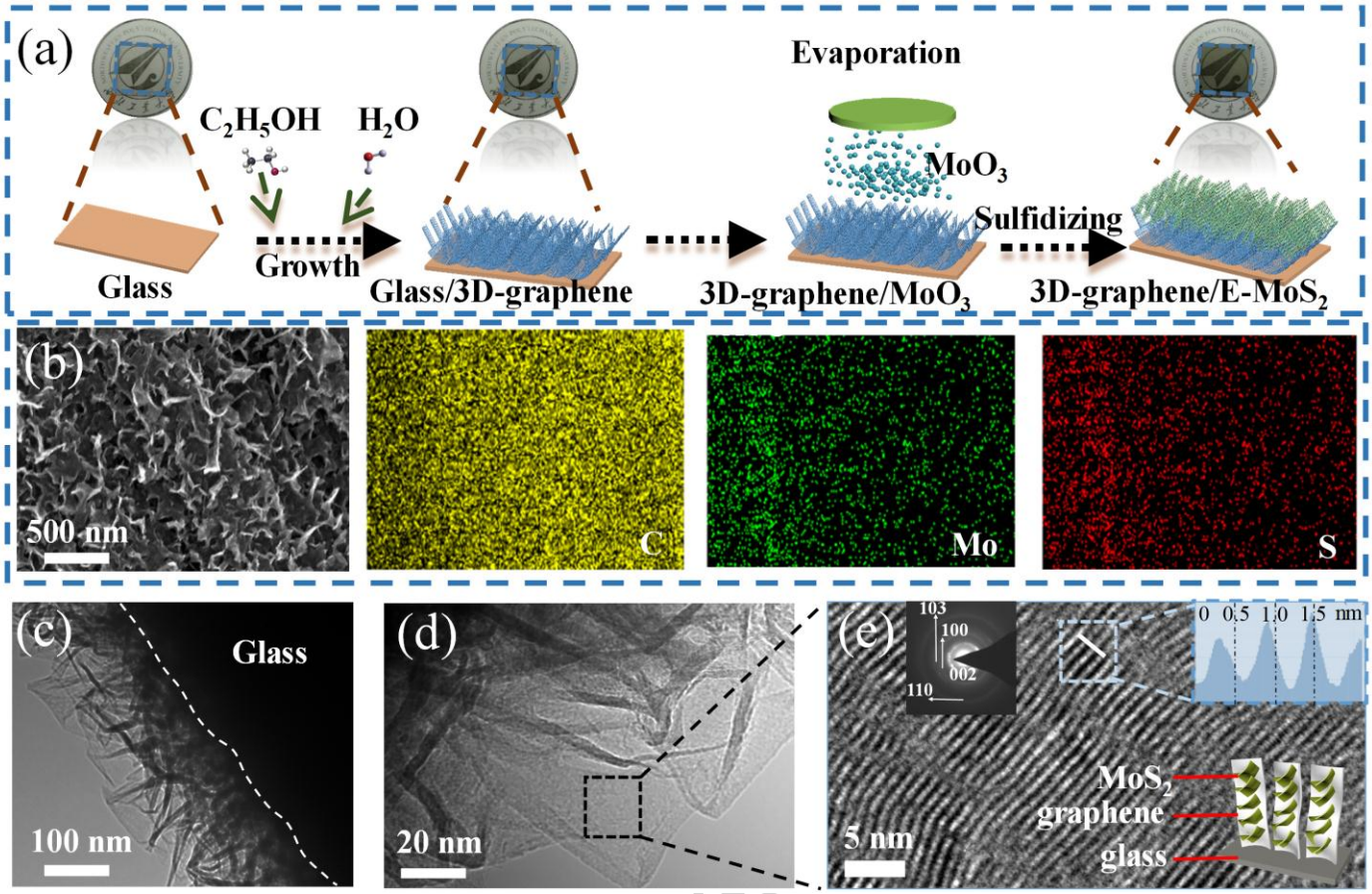

Fig. 1. (a) Schematic of the fabrication process of 3D-graphene/E-MoS_2. The background photos of samples are school badge of Northwestern Polytechnical University. (b) SEM image and elemental mapping images of 3D-graphene/E-MoS_2. (c) and (d) TEM images of 3D-graphene/E-MoS_2. (e) A magnified TEM image of 3D-graphene/E-MoS_2. The insets of (e) are a line profile taken from the white line (in (e)) with the MoS_2 lattice constant of 0.62 nm, the SAED of MoS_2, and a structured scheme of 3D-graphene/E-MoS_2, respectively.

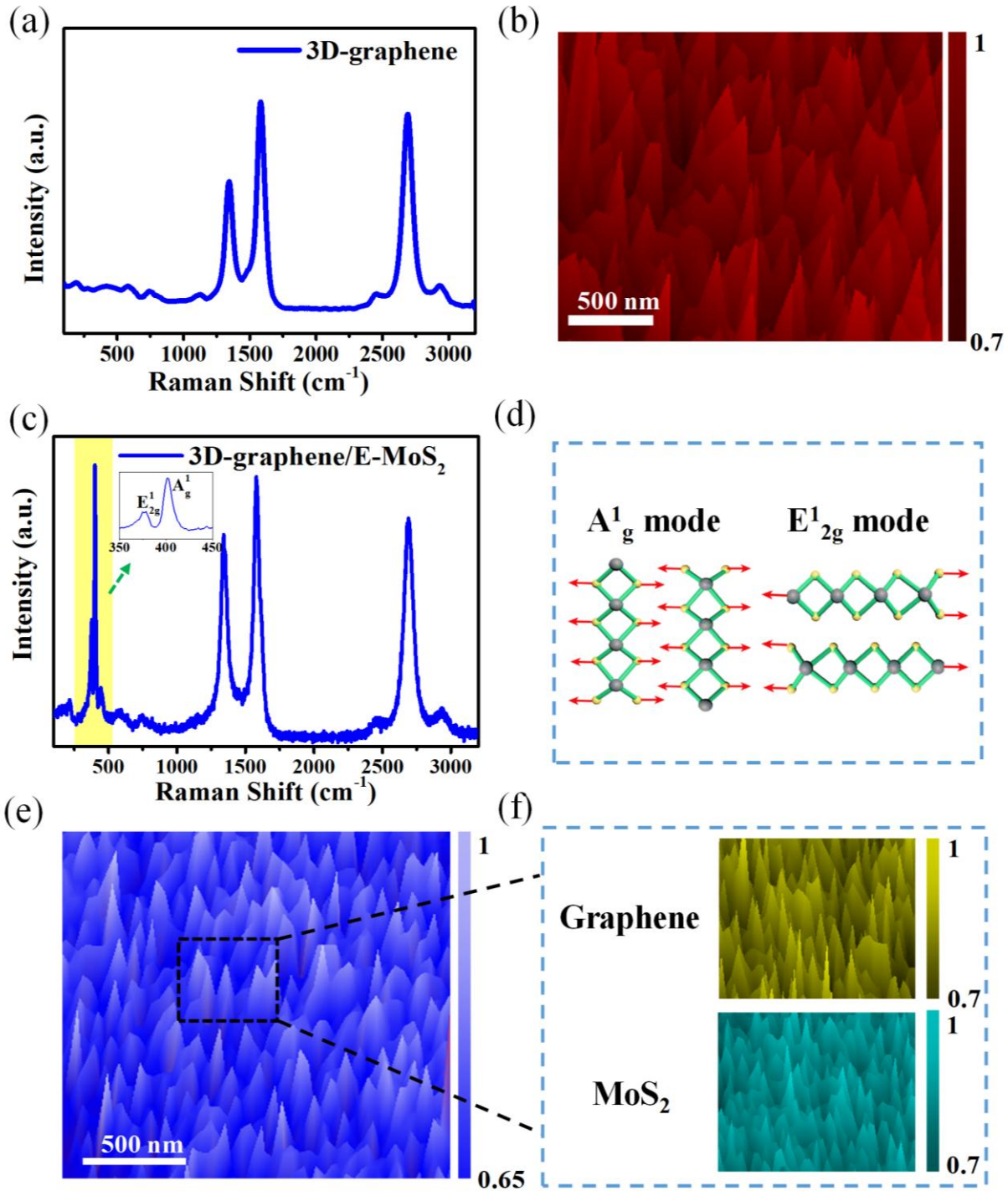

Fig. 2. (a) Raman spectrum of 3D-graphene. (b) Raman mapping image of the G band (1580 cm^{-1}) in the 3D-graphene sample and the Raman intensity is normalized. (c) Raman spectrum of 3D-graphene/E-MoS_2. The inset is the zoomed in part from the yellow region. (d) Schematics of preferentially excited A^1_g Raman mode for the edge-terminated film, and E^1_{2g} mode for the terrace-terminated film. (e) Raman mapping image of 3D-graphene/E-MoS_2 obtained from Raman components direct classical least squares (DCLS) analysis based on the reference spectra (pure3D-graphene Raman spectrum and pure E-MoS_2 Raman spectrum). The match between the reference spectra and the collected spectra is normalized to a value between 0.65 and 1, where values close to 1 indicate areas within the image with high similarities in

shape to that of the reference spectrum. (f) Raman mapping images of graphene and MoS_2 in the 3D-graphene/E-MoS_2 sample obtained from Raman Components DCLS analysis based on the pure 3D-graphene Raman spectrum and pure E-MoS_2 Raman spectrum, respectively. The match between the reference spectra and the collected spectra is normalized to a value between 0.7 and 1, where values close to 1 indicate areas within the image with high similarities to that of the reference spectrum.

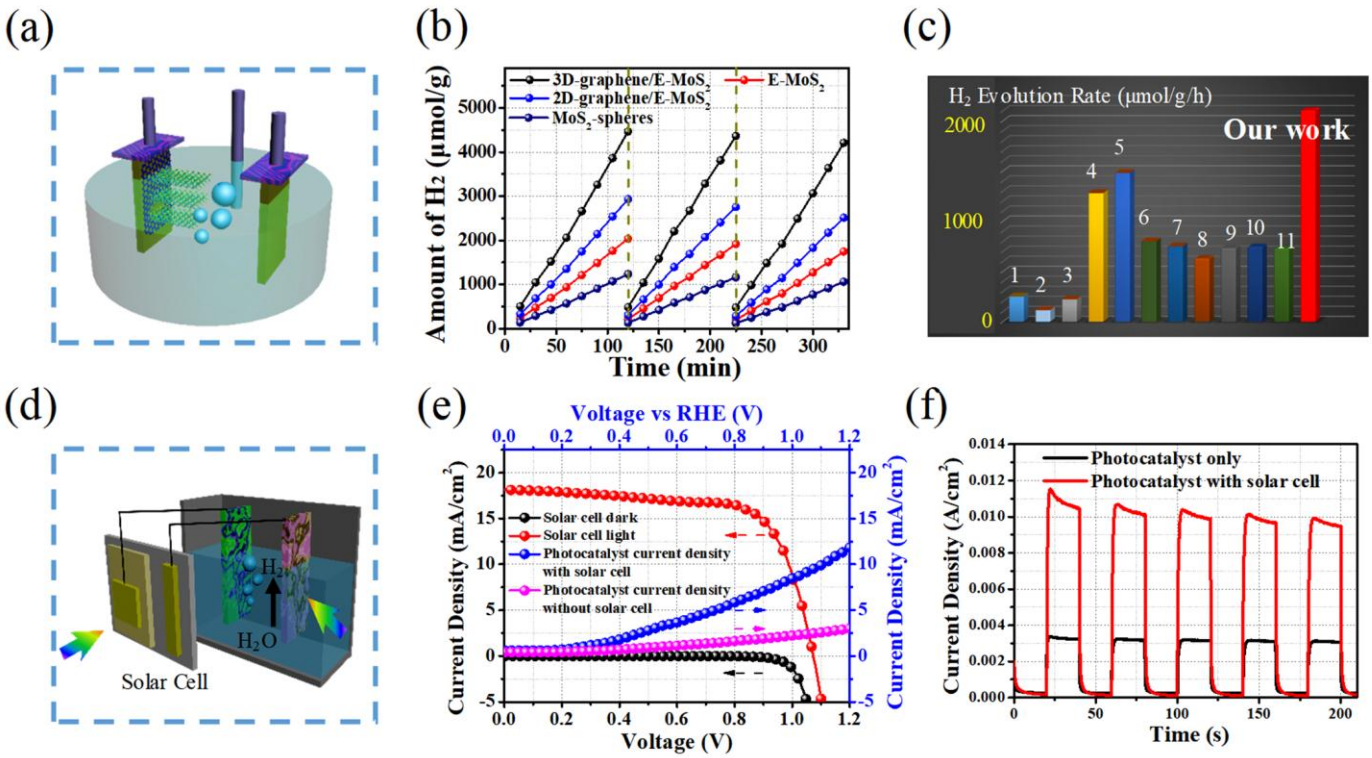

Fig. 3. (a) Schematic illustration of the photocatalysis activity measurement. (b) The photocatalytic activities of different MoS_2-based samples. (c) Photocatalysis-performance comparison of 3D-graphene/E-MoS_2 with the values of other photocatalysts in literature: (1) Sb-SnO_2, (2) CdS/Nb_2O_5/N-doped-graphene, (3) 5 wt% MoS_2 quantum dots/UiO-66-NH_2/graphene, (4) TiO_2/graphene, (5) g-C_3N_4, (6) g-C_3N_4/$Ca_2Nb_2TaO_{10}$, (7) phosphorus-doped C_3N_4, (8) T-C_3N_4, (9)g-C_3N_4, (10) Au@MoS_2-ZnO, and (11) Au multimers@MoS_2. (d) Schematic of the perovskite solar cell/photocatalysts parallel cell. The illuminated surface area of the photovoltaic (PV) cell is 0.22 cm × 0.22 cm (0.0484 cm^2). (e) The current density-voltage curve of the perovskite solar cell-photocatalyst parallel device under the standard AM 1.5G irradiation and in the dark. (f) The i-t curve of the parallel cell in 0.3 M Na_2SO_4 electrolyte under 1 Sun AM 1.5G (100 mW cm^{-2}) up to 200 s.

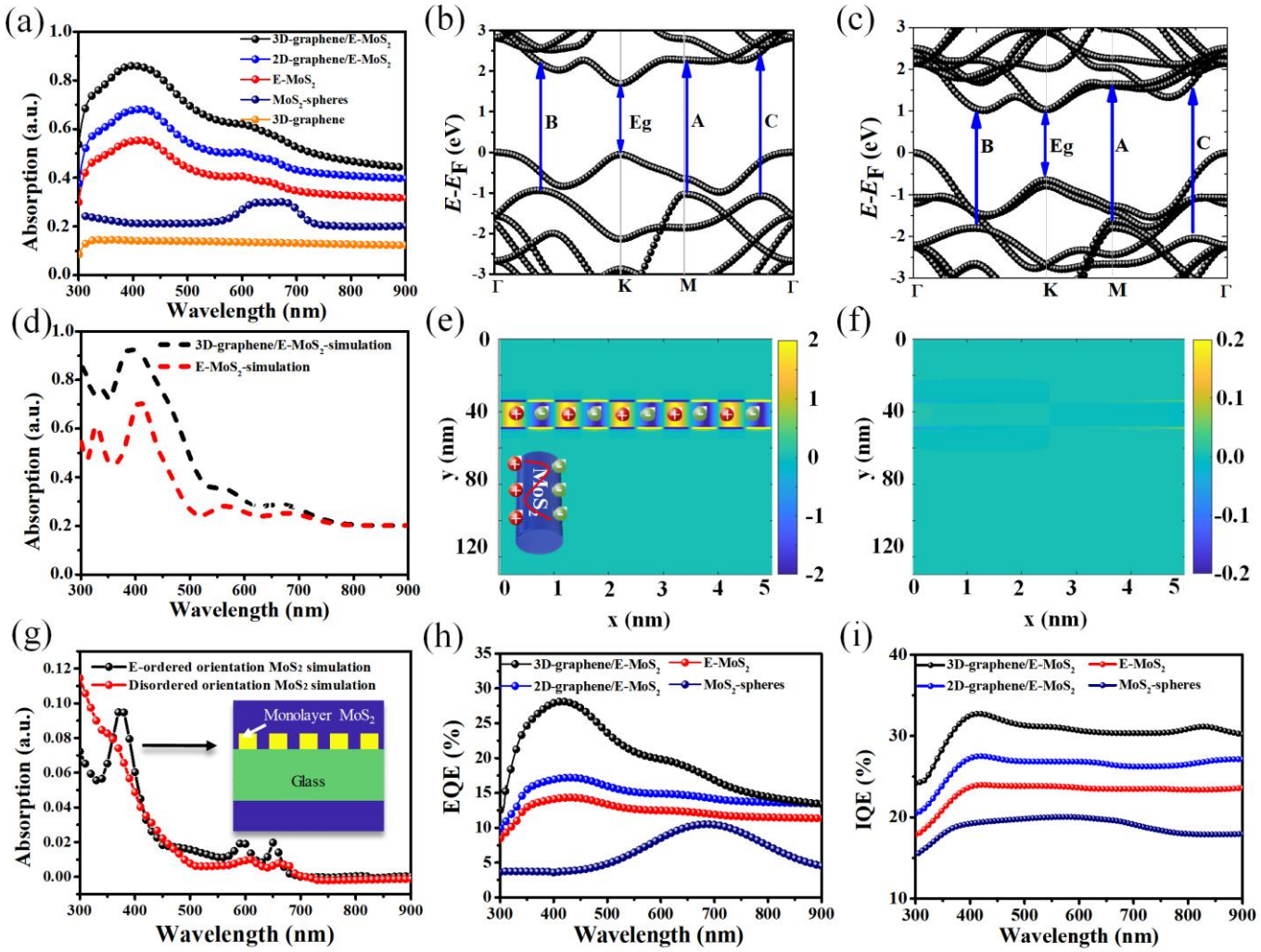

Fig. 4. (a) Experimental light absorption of samples. (b) Energy band of E-MoS_2. (c) Energy band of E-MoS_2 placed on top of the graphene. (d) Simulated light absorption of samples based on energy band. (e) Electrical field distribution of MoS_2 with an edge-ordered orientation. (f) Electrical field distribution of MoS_2 with disordered orientation. (g) Light absorption simulation based on the nanostructure. The inset is the schematic of the edge -ordered MoS_2 nanostructure. (h) EQE plots of samples, and (i) IQE plots of corresponding samples.

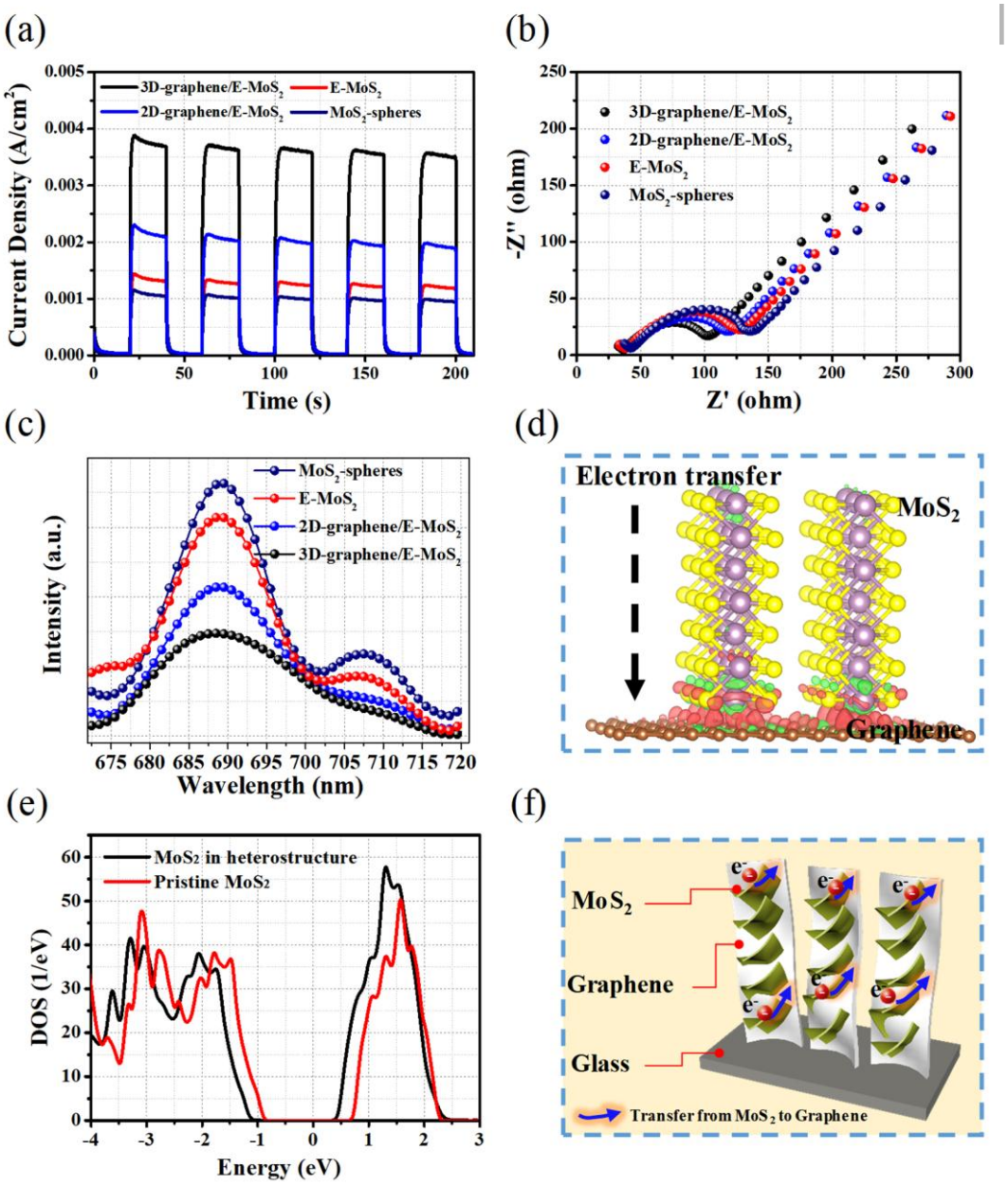

Fig. 5. (a) I-t curves, (b) EIS, and (c) PL of different samples. (d) The charge density difference at the interface of 3D-graphene/E-MoS_2. (e) The calculated total density of states of a pristine MoS_2 and the projected density of states for MoS_2 in the MoS_2-graphene nanostructure, and (f) schematic of charge transfer of 3D-graphene/E-MoS_2.

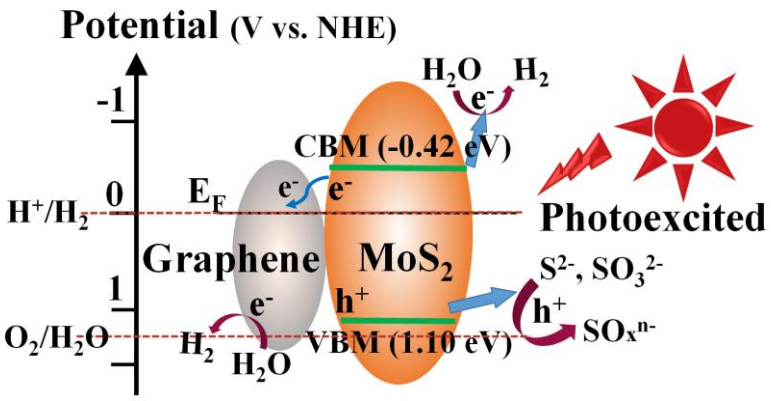

Fig. 6. Schematic of mechanisms of photocatalytic reaction.

Highlight

1. A conductive and transparent three-dimensional (3D) graphene is grown on a glass.
2. Edge-rich MoS_2 array grown on edge-oriented 3D graphene glass is rationally designed.
3. New finding in optical and electrical properties of the novel design is revealed.
4. One of the highest hydrogen evolution rates has been achieved based on the design.